An Overview of the Formation and Attitude Control System for the Terrestrial Planet Finder Formation Flying Interferometer

Daniel P. Scharf,* Fred Y. Hadaegh, Zahidul H. Rahman,
Joel F. Shields, and Gurkipal Singh
Jet Propulsion Laboratory, California Institute of Technology,
4800 Oak Grove Dr., Pasadena, CA 91109-8099 USA

The Terrestrial Planet Finder formation flying Interferometer (TPF-I) will be a five-spacecraft, precision formation operating near a Sun-Earth Lagrange point. As part of technology development for TPF-I, a formation and attitude control system (FACS) is being developed that achieves the precision and functionality associated with the TPF-I formation. This FACS will be demonstrated in a distributed, real-time simulation environment. In this paper we present an overview of the FACS and discuss in detail its constituent formation estimation, guidance and control architectures and algorithms. Since the FACS is currently being integrated into a high-fidelity simulation environment, component simulations demonstrating algorithm performance are presented.

I. Introduction

NASA's Terrestrial Planet Finder (TPF) mission will search for Earth-like planets orbiting other stars and probe their atmospheres for indications of life.[1,2] ESA's Darwin mission has similar goals.[3] TPF has baselined two architectures: an optical-wavelength coronagraph (TPF-C), and an infra-red formation flying interferometer (TPF-I). For TPF-I observations inter-spacecraft ranges and bearings must be maintained to 2 cm and 1 arcminutes, respectively, and attitudes must be maintained to within 1 arcminute. Hence, TPF-I is a precision formation. These performance requirements are derived from (*i*) the instrument requirement that the optical path difference between the arms of the interferometer be on the order of a nanometer (for nulling in the near-infrared) and (*ii*) system-level trades regarding active optics and optical delay lines.

To mitigate mission risk and advance formation flying technology, the TPF project has been developing several formation flying testbeds. In particular, the Formation Algorithms and Simulation Testbed (FAST) is a distributed real-time simulation environment that will demonstrate end-to-end operation of a formation flying mission with TPF-level functionality and precision. FAST will address formation complexity issues such as formation time synchronization, inter-spacecraft communication with latencies, inter-spacecraft sensing and data fusion, and system-wide formation robustness. Additionally, the FAST is responsible for developing a Formation and Attitude Control System (FACS) for demonstrating end-to-end precision formation flying operation of a preliminary TPF-I design. The specific hardware architecture, flight-like software executive, distributed simulation architecture, and initial results of the FAST are described in Ref. 5.

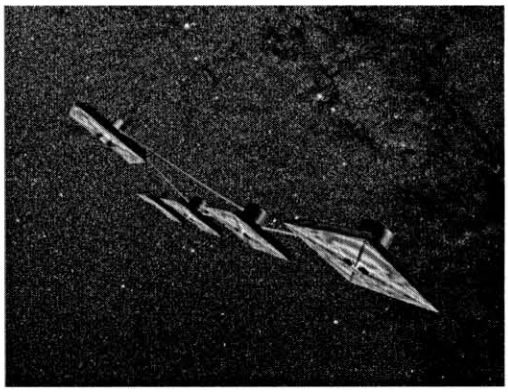

Figure 1. TPF Formation Flying Interferometer.

Formation control requires both traditional attitude control systems (ACS) and relative translational control systems. These two control systems are generally coupled. For example, estimating a relative spacecraft position requires the attitudes of two spacecraft. Combined attitude and relative translational control systems are referred to as a Formation and Attitude Control System (FACS).

*Corresponding Author. Email: Daniel.P.Scharf@jpl.nasa.gov, Phone:(818)-354-4795, Fax: (818)-393-0342

This paper describes the FACS being developed as part of the FAST for TPF-I technology demonstration. Specifically, we discuss the architectures and algorithms used for precision formation estimation, guidance and control of TPF-I, as well as the spacecraft dynamic models used for algorithm development and validation. In addition, we present preliminary performance results for these algorithms, which are currently being integrated into the FAST end-to-end, distributed real-time simulation environment. The performance of the formation in this high-fidelity simulation environment will be the subject of a future paper.

The remainder of this paper is organized as follows. First, we introduce the baseline TPF spacecraft design used for FACS development. Then the overall architecture of the FACS is discussed. Next, we present the architectures and specific algorithm designs for formation estimation, guidance and control in separate sections. Each section includes performance results based on stand-alone, component simulations. Finally, we present some conclusions.

II. Baseline TPF Spacecraft Design for Technology Development

The TPF-I flight design is still evolving. However, a fixed baseline technology design was created for FACS development. As the flight design continues to evolve, updates are integrated into the FACS baseline design consistent with the scope of the TPF formation flying testbeds. Moreover, the FACS is being designed to be adaptable to a number of flight designs. For example, the formation control architecture will function with the collectors in a line or at the corners of a square.

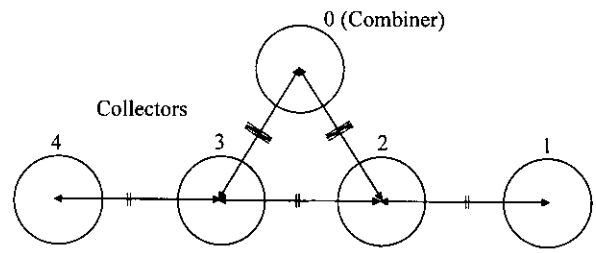

Figure 2. TPF Science Configuration.

While the FACS baseline design is not identical to the flight design, the baseline design has the important characteristics of the flight design. For example, the current sun-shield design is square while the FACS baseline sun-shield is round, but the salient feature for of the sun-shield for FACS is retained, namely, a fundamental mode of approximately 0.5 Hz. In the following we only present the details of the baseline spacecraft design important for FACS design, namely, mass and dynamic properties, actuators, sensors and inter-spacecraft communication.

Table 1. Baseline Design Mass & Dynamic Properties.

Property	Value
Mass	879 kg
I_{xx}	2787 $kg\,m^2$
I_{yy}	2836 $kg\,m^2$
I_{zz}	2266 $kg\,m^2$
Off-Diagonal Inertias	$< 1.5\%$ of I_{xx}
First Structural Mode	0.48 Hz
Modal Density	~70 per 5 Hz

The TPF formation consists of four Collectors and one Combiner. The Collectors are equally-spaced along a line. The Combiner forms an isosceles triangle with the two inner collectors. Spacecraft sun-shield separations range from 5 to 100 m. See Figures 1 and 2. Until a more mature Combiner design is available, we use five Collectors for FACS design. The addition of a Combiner will necessitate minor retuning of the FACS control and estimation algorithms, but no structural changes. The baseline Collector design is shown in Figure 3. Mass and dynamic properties are given in Table 1.

A. Actuators

Each spacecraft has 6-DOF uncoupled control authority via pulse-width modulated (i.e., constant force) thrusters. Reaction wheels are also available for attitude control. The thrusters are assumed to be configured to provide a minimum translational impulse of 0.5 $mN\,s$ and a minimum rotational impulse of 0.15 $mN\,m\,s$. The reaction wheels will be sized when the sun-shield design and observation maneuvers (e.g., formation rotation period) are finalized.

The baseline technology design mounts the thrusters on the spacecraft bus. The current flight design has the thrusters mounted on deployment arms. In the latter case, the control problem is not colocated.

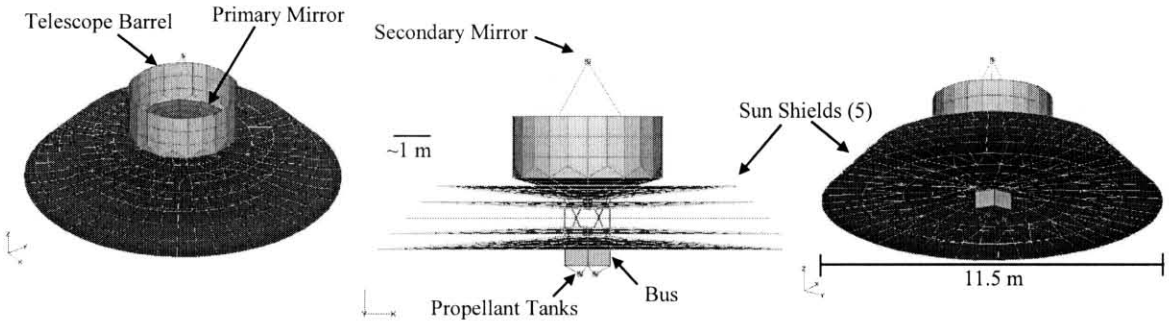

Figure 3. Baseline Collector Design for Technology Development.

However, the bandwidth of the FACS control loops is more than a decade below the fundamental frequency of the sun-shield/deployment arms, and so no problems are anticipated.

B. Sensors

For attitude estimation, each spacecraft is equipped with sun sensors, a gyro and two star-trackers. The second star-tracker is needed not for redundancy, but to reduce the measurement uncertainty about the boresight of the first. For relative translational estimation, each spacecraft has an accelerometer, and three relative sensing suites: acquisition, medium and fine. The medium and fine sensors have conical fields-of-view. The capabilities of each suite are given in Table 2.

Table 2. Relative Sensor Properties

Sensor	Range *km*	FOV[a] *deg.*	Range Acc. *cm* 1σ	Bearing Acc. *arcmin* 1σ
Acquisition	10	Full Sky	50	60
Medium	0.1	10	1	1
Fine	0.1	10	0.1	0.067

[a]Half-angle of conical field-of-view.

Each relative sensing suite has a different sensing topology. The acquisition sensor has an unlimited field-of-view (FOV): each spacecraft can measure the position of every other spacecraft, barring occultations. The medium and fine sensors have limited fields-of-view. Their sensing topologies are given in Figures 4 and 5, respectively. Since measurements are made on specific spacecraft, no spacecraft has local access to all the measurements necessary to produce a precision estimate of all the relative positions within the formation.

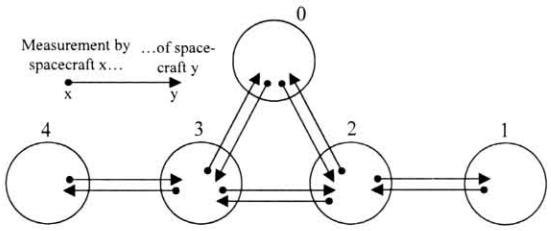

Figure 4. Medium Relative Sensor Topology.

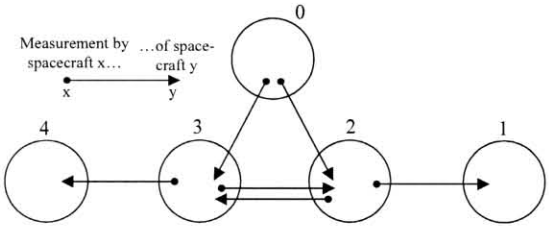

Figure 5. Fine Relative Sensor Topology.

C. Inter-Spacecraft Communication

Each spacecraft can communicate with every other spacecraft. The current flight design is to route communication through the Combiner. For nominal FACS design, however, the exact topology is not important as long as bandwidth is sufficient. For design, bandwidth is assumed sufficient for FACS needs.

During initialization of the formation, spacecraft clocks are synchronized to 20 *ms*. Due to the synchronization, it is possible to communicate information FACS in two windows. The communication windows are

discussed in the next section. Assuming direct point-to-point communication and no margin, a preliminary estimate of the peak bandwidth needed by FACS in these windows is 160 *kbps*. Further optimization of data size (e.g., floats vs. doubles) will reduce this number. The driving requirements, however, for TPF inter-spacecraft communication are the instrument control loops, which run at hundreds of Hertz. As a result, the current design of the TPF inter-spacecraft communication system supports 2 *Mbps*.

III. Formation and Attitude Control System Overview

The FACS contains all the elements of a general control system: an estimator to determine the values of the controlled variables, a path planner (referred to as guidance) to determine the desired values for the controlled variables, and a controller to drive the difference between the estimated and desired values to zero. In addition, a mode commander coordinates the different levels of functionality of the overall system. For example, guidance cannot begin to command a formation rotation until the estimator declares that relative position estimates are sufficiently accurate.

As much as possible, the FACS software is identical on each spacecraft. However, as discussed in the following sections, the Combiner serves as a leader for relative translational control and guidance. Additional functionality is activated aboard the Combiner by designating in software the Combiner as a leader and the Collectors as followers. It is possible to specify one of the Collectors as leader.

The FACS on each spacecraft runs at a rate of 1 Hz, resulting in a realtime time interval (RTI) of 1 *s*. This period is adjustable within limits. The estimation and guidance architectures discussed in the following sections require inter-spacecraft communication (ISC). Figure 6 shows both how the RTI is divided on each spacecraft and when ISC occurs. The numbers in the figure represent a fraction of RTI. All local sensors and commands from guidance, ground and mode commander are read by 0.1 RTI. By 0.2 RTI the first part of FACS, referred to as FACS1, has run. FACS1 includes the mode commander and the attitude estimator. Then the local quaternion and other information needed for relative translation estimation are communicated between spacecraft in the first communication window from 0.2 RTI to 0.4 RTI. Between 0.4 RTI and 0.75 RTI, the second part of FACS runs. This FACS2 includes the relative translation estimator, guidance and the attitude and controllers. Actuator commands are written to the actuator managers by 0.75 RTI. During the second communication window from 0.75 RTI to 1.0 RTI, mode commander and guidance information is communicated.

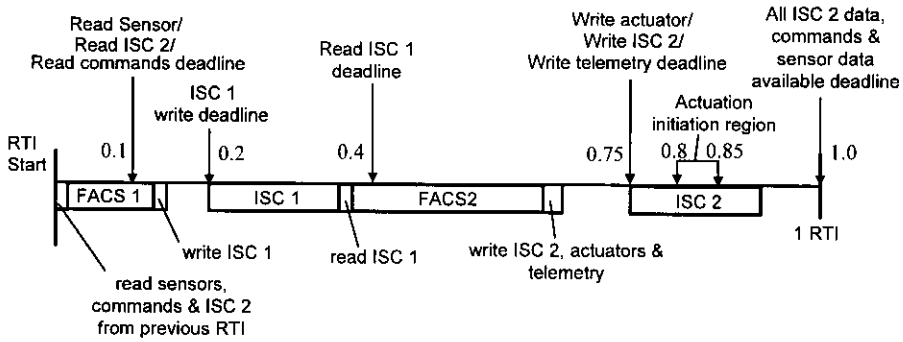

Figure 6. FACS Realtime Timing and Communication.

Finally, TPF-I performance requirements are the strictest during scientific observations. The formation must be rotated as a virtual rigid body and relative range and bearing controlled to 2 *cm* and 1 *arcmin* respectively, and attitudes to 1 *arcmin*. Since the sun-shields are 15.3 *m* in diameter, the 1 *arcmin* bearing requirement translates into a 6 *mm* position requirement at minimum spacecraft separations.

IV. Formation and Attitude Estimation

A. Estimation Architecture

The estimator must provide estimates of the controlled variables. As discussed subsequently in the Formation and Attitude Control Section, each spacecraft must control its inertial attitude, and each Collector must control the position of its center-of-mass (CM) with respect to the Combiner's CM. Attitude estimation is done in the standard way: each spacecraft makes its own measurements and estimates its own attitude.

In addition to the controlled relative position variable, we require each spacecraft to know the location of all the other spacecraft for collision avoidance monitoring and response. Furthermore, a centralized estimator that communicates this information to all spacecraft introduces a single point failure mode. Therefore, a decentralized relative translation estimation architecture is used for robustness. Each spacecraft estimates the positions of all other spacecraft CMs with respect to its own based on local measurements and on communicated measurements and data.

The communicated data consists of quaternion estimates and CM acceleration estimates. The CM acceleration estimates are needed to propagate the relative translational equations of motion. The CM acceleration estimates are produced by an Acceleration Data Processing algorithm onboard each spacecraft as discussed below.

One complication in relative translational estimation is that it is coupled one way to attitude estimation. Relative sensors provide measurements between sensor frames on respective spacecraft. However, since a CM-to-CM relative position vector is desired for control, the estimator must transfer from the two sensor frames (one on each spacecraft involved in the measurement) to CM-located body frames. This transfer requires the attitudes of both spacecraft.

For measurement based propagation (i.e., via accelerometer measurements), accelerometers and gyros are at 10 Hz. The star trackers and relative sensors provide measurements at 1 Hz. Propagation occurs at a faster rate to more accurately determine thruster cut-off times. The 10 Hz accelerometer and gyro measurements are stored and then processed in batch during FACS1 (see Figure 6).

B. Attitude Estimation Algorithm

The attitude estimator uses a Kalman filter that includes gyro bias states. Recall two star trackers are used. Star tracker measurement accuracies are 3 $arcsec$ 1σ about the transverse axes and 24 $arcsec$ 1σ about the boresight axis. Cassini-like gyro specifications were used to demonstrate the algorithm: an angle random walk variance of 5.3×10^{-13} rad^2/s^2, a rate random walk variance of 8.2×10^{-18} rad^2/s^3, and a correlation time of 100 s. Misalignments between the gyro and star tracker frames and the body frame are 10 $arcsec$. The performance of the attitude estimator is shown in Figure 7, which shows the difference between estimated and true angular positions about each body axis. The biases are due to the frame misalignments. Spacecraft attitudes are estimated to an average accuracy of 5.9 $arcsec$ 1σ, which is sufficient for attitude control. Detrended, the average performance of the estimator is 0.9 $arcsec$ 1σ.

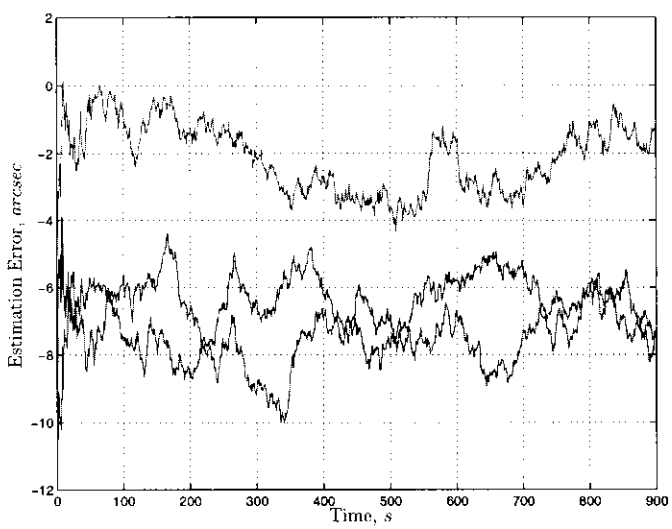

Figure 7. Attitude Estimation Error by Axis.

C. Relative Translation Estimation Algorithm

The relative translational estimator has two components: a Kalman filter and an Acceleration Data Processing (ADP) algorithm, which produces bias-corrected CM acceleration estimates.

We consider the Kalman filter first. Since the spacecraft are in deep space, the relative translational dynamics are modelled by double integrators.[6] As an example, Eqn. (1) is the propagation equation for spacecraft 4's estimator. The next two equations (2) and (3) are the measurement equations in terms of the state and in terms of the measured quantity. The measurement equations are for a medium sensor measurement between spacecraft 4 and 3 made onboard spacecraft 4. The state x is defined implicitly in (1):

$$\frac{d}{dt}\begin{bmatrix} x_{40}^I \\ x_{41}^I \\ x_{42}^I \\ x_{43}^I \\ \dot{x}_{40}^I \\ \dot{x}_{41}^I \\ \dot{x}_{42}^I \\ \dot{x}_{43}^I \end{bmatrix} = \begin{bmatrix} 0_{12x12} & I_{12x12} \\ 0_{12x12} & 0_{12x12} \end{bmatrix} \begin{bmatrix} x_{40}^I \\ x_{41}^I \\ x_{42}^I \\ x_{43}^I \\ \dot{x}_{40}^I \\ \dot{x}_{41}^I \\ \dot{x}_{42}^I \\ \dot{x}_{43}^I \end{bmatrix} + \begin{bmatrix} 0_{12x12} \\ I_{12x12} \end{bmatrix} \begin{bmatrix} a_0^I - a_4^I \\ a_1^I - a_4^I \\ a_2^I - a_4^I \\ a_3^I - a_4^I \end{bmatrix} + \begin{bmatrix} 0_{12x12} \\ I_{12x12} \end{bmatrix} \begin{bmatrix} w_{40} \\ w_{41} \\ w_{42} \\ w_{43} \end{bmatrix} \quad (1)$$

$$y = [0_{3x3}\ 0_{3x3}\ 0_{3x3}\ C(q_{B4}^{M43})C(q_I^{B4})\ 0_{3x12}]\,x + n_{43}^m \quad (2)$$

$$y_m = v_m + C(q_{B4}^{M43})r_{M43}^A - C(q_{B4}^{M43})C(q_I^{B4})C^T(q_I^{B3})r_{M43}^P \quad (3)$$

where the measurement is in the 4-to-3 medium relative sensor frame on spacecraft 4, x_{ij}^I is the position vector from spacecraft i's CM to spacecraft j's CM in the inertial frame, a_i^I is the inertial acceleration of spacecraft i's CM in the inertial frame, w_{ij} is the process noise for spacecraft j's CM position with respect to spacecraft i's, n_{ij}^m is the sensor noise for the medium measurement from spacecraft i to j, $C(q)$ is the rotation matrix corresponding to quaternion q, $q_I^{B_i}$ is the quaternion from inertial frame to spacecraft i's body frame, q_{B4}^{M43} is the quaternion from spacecraft 4's body frame to the medium sensor frame for the measurement from 4 to 3, v_m is the relative position measurement, r_{M43}^A is the position of the *active* portion of the medium measurement from 4 to 3 (i.e., where the measurement is made) on spacecraft 4 in spacecraft 4's body frame, and r_{M43}^P is the position of the *passive* portion of the medium measurement from 4 to 3 on spacecraft 3 in spacecraft 3's body frame. Clearly, some careful bookkeeping is necessary.

Eqn. (3) illustrates the attitude coupling of the relative translation estimator. The quaternions q_I^{B4} and q_I^{B3} are provided by the attitude estimators on spacecraft 4 and 3, respectively. The quaternion q_I^{B3} must be communicated from spacecraft 3. Spacecraft 4 must also have a database containing the characteristics of spacecraft 3's sensor hardware. In this case, values for $r_{M43_P}^P$ and q_{B3}^{M43} must be stored. Similarly, to propagate the equations of motion (1) the accelerations a_i^I, $i = 0, 1, 2, 3$ must be communicated to spacecraft 4. As a last comment, relative measurements in which spacecraft 4 is not involved are also be included. For example, a medium sensor measurement between spacecraft 2 and 0 can be represented by $x_{40}^I - x_{42}^I$. In the case where the measurement is made onboard spacecraft 2, Eqn. (2) would be replaced by

$$y = [C(q_{B2}^{M20})C(q_I^{B2})\ 0_{3x3}\ \ -C(q_{B2}^{M20})C(q_I^{B2})\ 0_{3x3}\ 0_{3x12}]\,x + n_{20}^m\,.$$

In Eqn. (1), the inertial CM accelerations a_i^I are calculated by the Acceleration Data Processing (ADP) algorithm aboard each spacecraft i and then communicated to all other spacecraft. The ADP consists of another Kalman filter for estimating the accelerometer bias, which consists of a constant term plus a random walk. The ADP also converts the acceleration measured by the accelerometer, which is not located at the CM, to the equivalent acceleration at the CM using gyro measurements. The quaternion estimate is used then to transform the acceleration from body frame to inertial frame.

A challenge in relative translational propagation is that the thrusters are very small (e.g., 50 mN). As a result, for minimum on-time thruster firings the accelerometer SNR can be very small. If the accelerometer measurement magnitude is below a threshold, then the ADP uses commanded thruster on-times to generate

the effective acceleration using thruster models. This model-based acceleration approach provides more accurate acceleration estimates than low SNR accelerometer measurements.

Combining the ADP and the relative translational Kalman filter produces the full relative translational estimator. The performance of the estimator was demonstrated in a 700 s simulation during which spacecraft 4 maneuvered to bring different relative sensors into lock. Figure 8 shows the estimation error of spacecraft 4's estimate of spacecraft 3's relative position. The simulation includes sensor-to-body frame misalignments of 10 $arcsec$ and sensor location uncertainties of 0.1 mm (recall r^A_{M43} in (3)). The simulation includes the attitude estimator and so attitude estimation errors are included. In Figure 8(a), the acquisition sensor is locked at the beginning. As can be seen, estimation errors are consistent with a 50 cm measurement error (see Table 2). At 270 s, the medium relative sensor locks, and the estimation error is reduced to less than 1 cm. Figure 8(b) shows the performance during medium and fine lock with a finer ordinate scale. With the fine sensor locked, relative positions are estimated to an average accuracy of 1.7 $mm\,1\sigma$, which is sufficient for the 6 mm control performance requirement. The biases apparent in Figure 8(b) are due to frame misalignments and sensor location uncertainties. Transforming to range and bearing, the average range performance is 0.13 $mm\,1\sigma$ and the average bearing performance is 0.14 $arcmin\,1\sigma$.

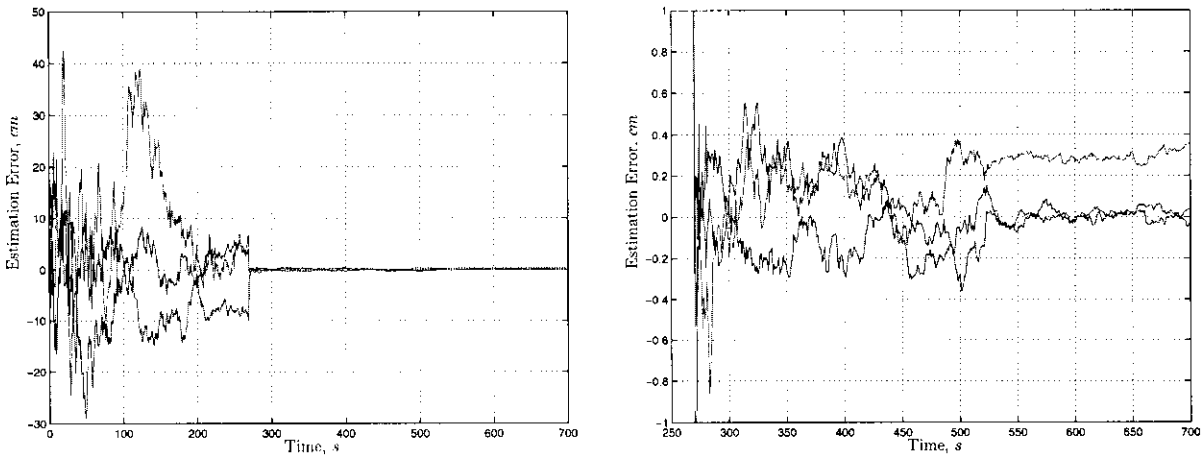

(a) All Relative Sensing Stages: Acquisition Lock at 0 s, Medium Lock at 270 s, Fine Lock at 522 s.

(b) Detail of Performance with Medium and Fine Relative Sensors.

Figure 8. Relative Translation Estimation Error by Axis.

V. Formation and Attitude Guidance

A. Guidance Architecture

The formation guidance provides reference trajectories to the formation and attitude controllers. As such, the output of the formation guidance depends on the particular control architecture. As discussed subsequently in the Formation and Attitude Control section, attitudes are controlled independently and the relative positions are controlled via a Leader/Follower architecture. For attitude control, the formation guidance calculates desired quaternions, angular velocities and angular accelerations. For relative position control, the formation guidance calculates the desired position and velocity of each Collector (Follower) relative to the Combiner (Leader) and open-loop inertial acceleration profiles for all spacecraft.

For TPF-I there are three mission phases: Formation Acquisition, Formation Reconfiguration, and Observation. Formation acquisition, also known as formation initialization, is the process of obtaining relative dynamic state information and establishing communication. It occurs after deployment or a fault condition. Formation reconfiguration moves the formation from one configuration to a new configuration. Reconfigurations occur after acquisition to move the formation to its initial science configuration, and after a science observation to retarget. Finally, the observation phase consists of rotating the formation as a rigid body

and changing its baseline (i.e., the distance between spacecraft 1 and 4 in Figure 2) to synthesize a synthetic aperture. The observation phase is unique in that spacecraft attitudes must be synchronized with relative positions for the interferometer to operate.

In each of these three phases formation guidance must command the formation, that is, provide attitude and relative translation paths for all the spacecraft.

A hybrid architecture was selected for the formation guidance. Relative translational paths are centrally planned onboard the Combiner, while attitude planning is decentralized. Specifically, attitude paths are planned locally based on high-level commands from the Combiner, for example, a final attitude and a final time. The relative translational guidance was centralized to ensure formation-wide constraint satisfaction and to reduce the complexity of synchronizing relative positions and attitudes during precision formation rotations.

In contrast to the estimation architecture, there is no robustness issue with centralized relative translational guidance. If a serious fault disables the Combiner, all the spacecraft default to a stand-alone, safe stand-off mode where each spacecraft is responsible for its own collision avoidance. This stand-off mode is possible because the formation estimation is decentralized.

There are three main constraints that the attitude and relative translational paths must satisfy: the collision avoidance constraint (CAC), the sun avoidance constraint (SAC), and the relative thermal constraint (RTC). For the CAC, exclusion spheres are placed around each spacecraft, and relative translational paths must not cause the spheres to intersect. The SAC protects the infra-red optics. It requires the payload "boresights" to remain within a cone about the anti-sun line. See Figure 9.

Finally, recall that TPF-I is an infra-red interferometer. The optics are cooled to 40 K. The hot side of each spacecraft's sun-shield is approximately 300 K. If the hot side of one spacecraft's sun-shield were to illuminate the cold optics of another it would heat the optics. Then the formation would have to sit idle while the optics re-cool to $40K$. For each spacecraft, the RTC requires that relative position vector to the other spacecraft remain approximately 85 *deg* or more away from the sun-shield normal. The RTC is a time-varying attitude constraint that depends on the relative positions of the formation.

B. Attitude Guidance Algorithm

The attitude guidance algorithms onboard each spacecraft are extensions of the attitude guidance algorithm designed for the Cassini mission.[7] On each spacecraft a base frame is defined by aligning (i) a body fixed direction with an inertial direction and (ii) a second body fixed direction as much as possible with a second inertial direction. Attitude turns are then commanded by specifying a new attitude relative to either the current or base frame.

When a new attitude is commanded, the guidance first checks if the new attitude violates the SAC. If it does, the command is rejected. If not, then an attitude path is first planned based on an Euler turn. If during this turn the SAC is violated, then turn broken into three Euler turns that do not violate the SAC.

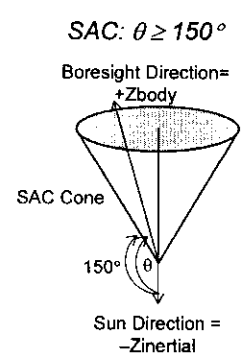

Figure 9. Example Sun Avoidance Constraint.

As an example of SAC satisfaction by the attitude guidance, consider Figure 9. The +Z body axis is the payload boresight of a Collector. In this example, the boresight must remain within 30 *deg.* of the anti-sun line, which is the +Z inertial axis. Per the guidance interface, this is equivalent to maintaining the angle θ between the -Z inertial axis and the +Z body axis greater than 150 *deg.*

Figure 10 shows the guidance replanning to satisfy the SAC by plotting θ versus time. First a rotation about the +X inertial axis places the boresight axis near the edge of the SAC cone. Then a 170 *deg.* turn is commanded. If one Euler turn is used, the SAC is violated. However, the attitude guidance detects this violation and replans three smaller turns that all satisfy the SAC.

Recall that during the observation phase, attitudes must be synchronized with spacecraft relative positions. This synchronization is accomplished by continually specifying the second inertial direction of the base frame to be the rotating baseline direction. In this case, attitude and translational guidance is centralized,

since the baseline direction is updated each RTI by the Combiner. Alternatively, to maintain decentralized attitude guidance, the second inertial direction can be assigned to be the vector to a neighboring spacecraft. Then each spacecraft would estimate this vector and calculate attitude commands individually.

C. Relative Translation Guidance Algorithms

We consider each of the three mission phases. For formation acquisition, recall that the acquisition sensor has an unlimited FOV. See Table 2. Further, the baseline TPF-I design includes omnidirectional communication. As a result, formation acquisition consists of turning these systems on. If communication and relative sensing are not immediately established, two probable causes are a failure or an occultation. The deployment of the spacecraft from the cruise stage can be planned to avoid occultations. In the event of an antenna failure of the full-sky acquisition sensor, the limited-FOV acquisition algorithm of Ref. 8 can be used. Another possibility may be that the spacecraft are separated beyond the range of the acquisition sensor. In this case, ground intervention is needed.

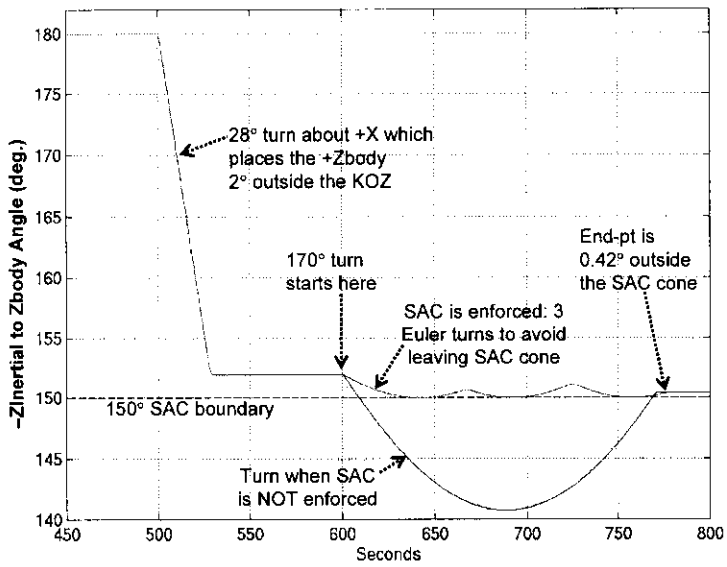

Figure 10. Example of Attitude Replan to Enforce SAC.

For formation reconfiguration, a general deep space, energy-optimal formation reconfiguration algorithm with collision avoidance has been developed.[9] This algorithm does not address the RTC. However, the RTC is only active after the spacecraft have cooled to 40 K. Therefore, after formation acquisition, the algorithm of Ref.[9] is used to plan trajectories to move the formation from its post-acquisition configuration to the initial science configuration.

One the formation has assumed the science configuration and cooled, the RTC is active. Reconfigurations are then needed to retarget the formation between observations. Planning coupled relative translation/attitude reconfigurations with an RTC is an open area of research. Therefore, for retargeting reconfigurations we rotate the formation as a virtual rigid body. This approach satisfies the CAC and RTC, and avoids communication and sensor occultations. Finally, since the initial baseline direction for a new science target is unconstrained, an Euler rotation of the formation, in which the individual spacecraft behave as if embedded in a virtual rigid body, can always be found that satisfies the SAC for the spacecraft.

To illustrate, consider Figure 11. In science configuration, each spacecraft aligns its payload boresight (body z-axis) with the formation boresight $\vec{s}$. The Collectors must also be aligned along the current baseline vector $\vec{b}$ with their body x-axes aligned with the baseline. When an initial baseline for Target 2 is specified, an Euler retargeting rotation can cause the aperture boresights to leave their SAC cones. However, when the initial baseline for Target 2 is free, an Euler rotation can always be found that satisfies the SAC during the entire retargeting. If a future mission operational design constrains the initial baseline for a new target, then a sequence of three Euler rotations can be found to satisfy the SAC as in Figure 10. The algorithm for formation rotations is discussed in more detail as part of the observation phase.

We conclude the formation guidance section with formation observations. For observations the formation must be rotated about the formation boresight vector and attitudes must be synchronized with relative positions. For retargeting the formation can be rotated about an arbitrary axis and there is no attitude/relative position synchronization requirement. As a result, the same relative translational guidance algorithm is used for both observation and retargeting rotations. Synchronized attitudes are achieved by commanding each spacecraft to align its body z-axis with the formation boresight and either (i) its body x-axis with the

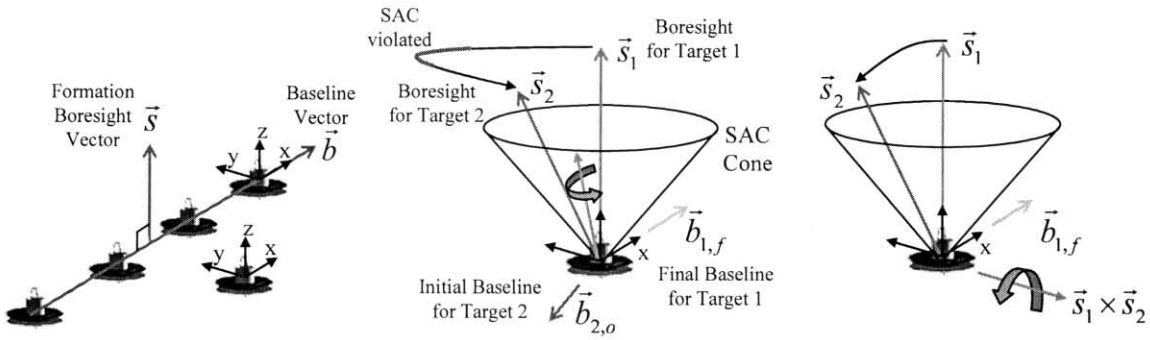

a) Formation Science Geometry. For rigid rotations, aperture boresights (z) are identical to the formation boresight.

b) When the initial baseline is specified for the next target, an Euler formation rotation can violate the SAC.

c) When the initial baseline for next target is free, an Euler formation rotation can be found that meets the SAC.

Figure 11. Satisfaction of SAC During Formation Retargeting via Rotation.

baseline vector or (*ii*) an assigned body vector with the direction to a neighboring spacecraft.

A formation rotation algorithm has been developed that rotates the formation about the energy-optimal point. The spacecraft travel on a polygonal approximation to arcs, where the number of polygonal segments is commandable. For a two-spacecraft Combiner/Collector formation, Figure 12 shows a 4-segment 180 *deg.* formation rotation followed by two 90 *deg.* rotations of increasing segments. The relative position is shown in a frame attached to the Combiner. The Combiner does move: it follows an open-loop acceleration profile. In this example, attitudes are synchronized even for rotations that are not about the boresight vector. Figure 13 illustrates this synchronization by showing the angular rate command for the Collector.

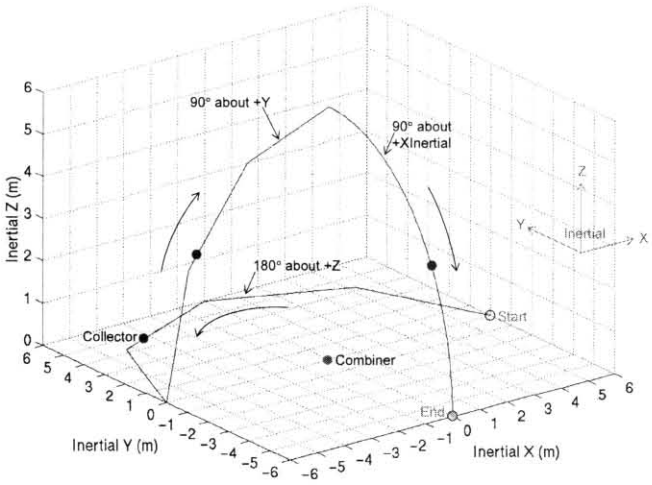

Figure 12. Example Formation Rotation Maneuvers.

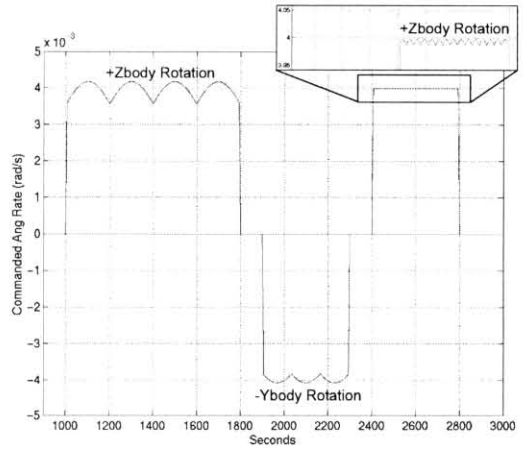

Figure 13. Attitude Synchronization During Rotations.

VI. Formation and Attitude Control

A. Control Architecture

For TPF-I technology demonstration we selected the Leader/Follower (L/F) decentralized control architecture for controlling relative spacecraft positions.[10] The L/F architecture is robust (e.g. individual spacecraft failures do not affect the overall stability of the remaining formation), scalable (e.g. spacecraft can be easily added using only local control design), and has deterministic communication requirements. The stability properties of the L/F architecture are also well understood. In particular, for homogenous Followers, L/F al-

lows one relative controller to be designed, and this design copied by each Follower. For TPF-I, the Combiner is the Leader, and each Collector follows it.

Attitude control (as opposed to guidance) is uncoupled to relative translational control. Therefore, independent attitude controllers can be designed. Attitude control is completely decentralized.

In operation, each Collector estimates its relative position with respect to the Combiner and its inertial attitude. Based on relative translational guidance from the Combiner and local attitude guidance, each Follower's controllers drive performance errors to within the requirements. The Combiner controls its attitude and applies feedforward accelerations as dictated by formation guidance.

There is an important, non-standard constraint on relative position and attitude control. Observations are performed entirely using thrusters. Since the thrusters are not throttleable, their firing can cause spacecraft vibrations that interrupt the interferometer. To allow for both actuation and science, all thrusters on all spacecraft for both attitude and relative position control may only fire in a 6 s window every 54 s. Data gathering occurs during the 54 s between thruster firings. This requirement is referred to as the thruster synchronization constraint (TSC).

B. Formation and Attitude Control Algorithms

For control design, both the relative translational and the attitude dynamics are well approximated by independent double integrator models. Relative translational control design is simplified since TPF-I will be in orbit about a Sun-Earth Lagrange point. In these orbits, the relative translational dynamics are well approximated by decoupled double integrator models.[11] Similarly, since the TPF spacecraft are three-axis stabilized, have small off-diagonal inertias, and rotate slowly, the small angle approximation is valid. In this approximation, the quaternion is decomposed into independent body axis angle errors, and the dynamics of each angle error are approximated by a double integrator model. Since each relative translational and rotational degree of freedom is modelled by a double integrator, one SISO controller can be designed for all degrees of freedom and then scaled to the correct double integrator model (e.g., by multiplying by the inertia about a principal axis).

For control design, we used a classical approach augmented with nonlinear dynamic compensation.[12] The controller is divided into two parts: a fast controller that runs at the 1 Hz FACS rate, and a slow controller that runs at 0.25 Hz. The slow controller has a sample period of 4 s to provide margin in the 6 s RTC window. While the slow controller runs at 0.25 Hz, its output is ignored except at the beginning of each 6 s window. Both controllers are stable individually and in parallel. Switching between the fast and slow controllers is done using nonlinearities in the controller, and so no additional mode commander is necessary. The nonlinearities enforce the phase space logic shown Figure 14. As can be seen, the fast controller turns off when the position tracking error is small. Then actuation only occurs every 56 seconds per the RTC. Also note that there are regions of the phase space where no control is active. The current design is such that the maximum drift time is 17 s. These regions could be removed at the cost of increased controller complexity, but the regions do not affect tracking performance.

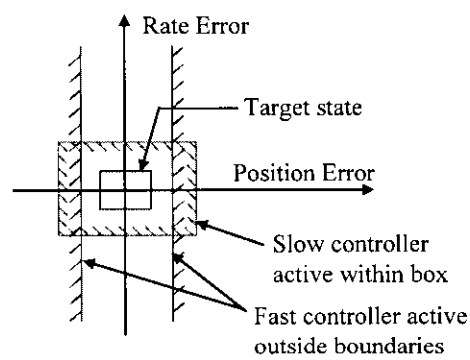

Figure 14. Phase Space Switching between Fast and Slow Controllers.

The fast controller is a PD with nonlinear dynamic compensation, and it includes rate saturations in the event of large tracking errors. The slow controller is a PID with nonlinear dynamic compensation. The slow controller includes is a PD controller, also with nonlinear dynamic compensation. The nonlinear compensation in both the fast and slow controllers allows a conditionally stable loop to be designed that is stable in the event of saturations. In effect, high gain controllers have been designed based on the Bode integral constraints that reduce their gain as tracking errors become large.[12]

The control design was simulated to demonstrate its performance. Figure 15 shows the results for one such simulation. The scenario considered was the attitude control of a Collector during observation. Recall that during observation the formation is rotating about the formation boresight which corresponds to the body z-axes of the spacecraft, and that spacecraft attitudes are synchronized to relative positions. Hence,

the spacecraft rotate at a constant rate about their body z-axes.

The dynamic model used in the simulation includes the sun-shield dynamics, which have a fundamental mode at 0.5 Hz. The upper left plot shows the angle and angle rate about the body z-axis. Also shown are the thruster firings and the 6 s firing windows of the TSC. These last two are seen more clearly in the lower left plot, which shows them in the steady state (note the range of the abscissa). As can be seen, the thrusters only fire in the allowable windows. The upper and lower plots on the right of Figure 15 show the angle and angle rate error about the body z-axis. The vibrations visible in the angle rate error are due to the sun-shield dynamics. Also, the transient will be reduced when the controllers are integrated with the formation guidance, which provides feedforward accelerations. As can be seen from the figures, the performance requirements are met for attitude control. Similar simulations have shown that the relative translational performance requirements are also met.

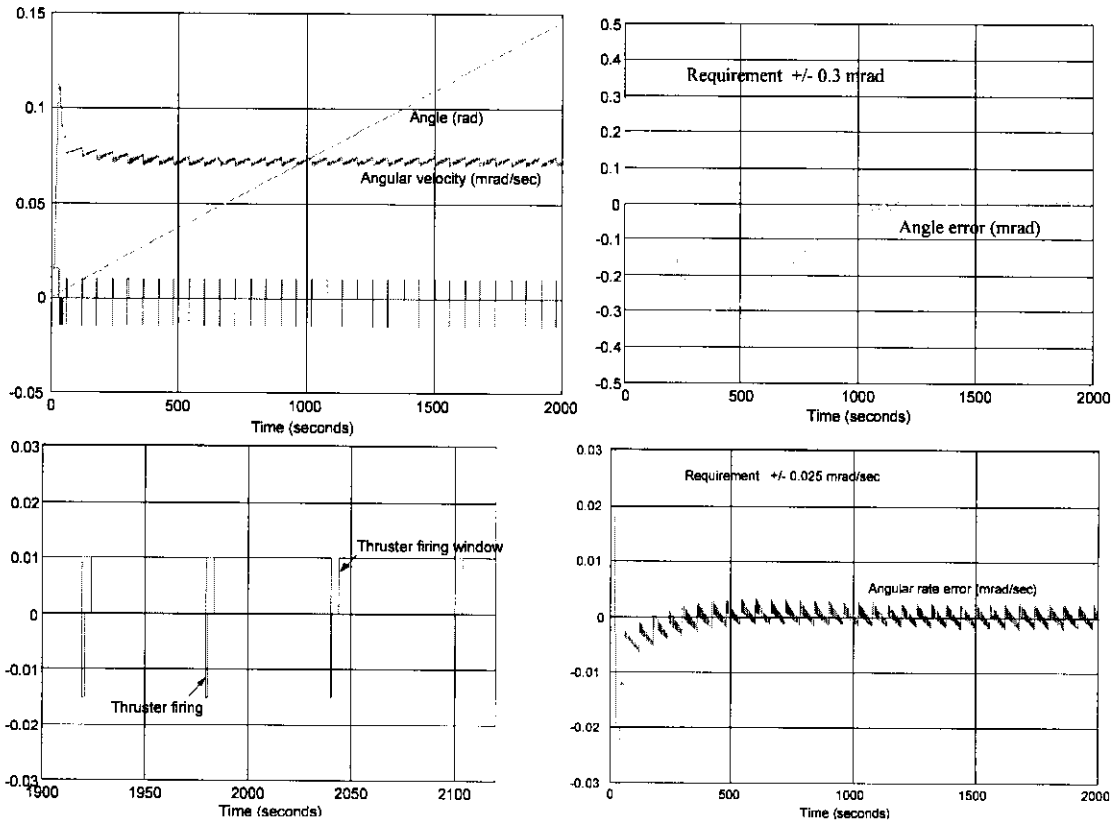

Figure 15. Attitude Control Performance with RTC.

VII. Conclusions

We have introduced the Formation and Attitude Control System (FACS) being developed as part of the TPF project for demonstrating long-term precision formation performance and robustness. We first discussed the spacecraft dynamic model, which has a fundamental sun-shield mode at approximately 0.5 Hz, the actuators, and the various sensor suites and topologies. Then each element of the FACS, estimation, guidance, and control, was discussed in detail. The guidance provided desired relative positions to each of the Collectors and desired attitudes during each of the three formation phases. The non-standard, coupled attitude/position relative thermal constraint (RTC) was addressed via formation rotations. The estimator and controller combined to achieve the 2 cm and 1 $arcmin$ performance requirements. The controller incorporated the thruster synchronization constraint (TSC) by having a fast and a slow controller and nonlinear dynamic compensation. The estimator, in which relative position estimates are coupled to attitude

estimates, includes an acceleration data processing unit to account for low SNR accelerometer measurements and biases. The estimator also drives the inter-spacecraft communication requirements for FACS.

The FACS is currently being integrated into the distributed, real-time simulation environment of the Formation Algorithms and Simulation Testbed (FAST). The stand-alone, component simulation results reported in this paper will then be validated in that high-fidelity simulation testbed. Results from these simulations as well as formation fault responses and the formation mode commander, which coordinates the high-level functionality of the FACS, will be the subjects of a future paper.

Acknowledgments

This research was performed at the Jet Propulsion Laboratory, California Institute of Technology, under contract with the National Aeronautics and Space Administration.

References

[1]Beichman, C., Woolf, N., and Lindensmith, eds., C., "The Terrestrial Planet Finder (TPF):A NASA Origins Program to Search for Habitable Planets," JPL Pub. 99-3, Cal. Inst. Tech., Pasadena, CA.

[2]Lawson, P., "The Terrestrial Planet Finder," *IEEE Aero. Conf.*, 2001, pp. 2005–2011.

[3]Fridlund, C., "Darwin—the Infrared Space Interferometry Mission," *ESA Bulletin*, Vol. 103, 2000, pp. 20–63.

[4]Lagadec, K., Lebas, J., and Ankersen, F., "GNC System for the Control of the Darwin Free-Flying Interferometer," *Int. Symp. on Formation Flying Missions & Technologies*, Toulouse, France, 2002.

[5]Wette, M., Sohl, G., Scharf, D., and Benowitz, E., "The Formation Algoriths and Simulation Testbed," *Int. Symp. Formation Flying Missions & Technologies*, Washington, D.C., 2004.

[6]Scharf, D., Hadaegh, F., and Kang, B., "On the Validity of the Double Integrator Approximation in Deep Space Formation Flying," *Int. Symp. Formation Flying Missions & Technologies*, Toulouse, France, 2002.

[7]Rasmussen, R., Singh, G., Rathbun, D., and Macala, G., "Behavioral Model Pointing on Cassini Using Target Vectors," *Annual AAS Guid. & Contr. Conf.*, 1995.

[8]Scharf, D., Ploen, S., Hadaegh, F., and Sohl, G., "Guaranteed Spatial Initialization of Distributed Spacecraft Formations," *AIAA Guid., Nav., & Contr. Conf.*, 2004.

[9]Singh, G. and Hadaegh, F., "Collision Avoidance Guidance for Formation-Flying Applications," *AIAA Guid., Nav., & Contr. Conf.*, 2001.

[10]Wang, P. and Hadaegh, F., "Coordination and Control of Multiple Microspacecraft Moving in Formation," *J. Astro. Sci.*, Vol. 44, No. 3, 1996, pp. 315–355.

[11]Gómez, G., Lo, M., Masdemont, J., and Museth, K., "Simulation of Formation Flight Near Lagrange Points for the TPF mission," *AAS/AIAA Astro. Conf.*, 2001.

[12]Lurie, B., "Multi-mode Synchronized Control for Formation Flying Interferometer," *AIAA Guid., Nav., & Contr. Conf.*, 2003.